A High-Efficiency Integrated Converter for LED Driver

Omid Honarfar¹, Abbas Ketabi¹* iD

¹Department of Electrical and Computer Engineering, University of Kashan, Kashan, Iran
E-mail: aketabi@kashanu.ac.ir

Abstract—Enhancing the efficiency in the light-emitting-diode (LED) drivers is a noteworthy issue as it not only helps saving energy but also causes the long life span of the drivers. In this paper, a new LED driver with improved efficiency is proposed. Efficiency improvement is achieved without using any active or passive component to perform soft switching conditions. In the proposed driver, buck and buck-boost converters are integrated. The freewheeling diodes and inductors - of the two converters - are replaced by one diode and one inductor. So, the proposed driver constitutes a single-stage driver with a simple structure that uses only one controlled switch, one freewheeling diode, and one inductor. Besides its simple structure, the driver works with a constant frequency, which leads to using a simple controller. Efficiency improvement is obtained by changing the inductor size and LEDs arrangement rather than using the active clamp or snubber circuits. To decrease the switching losses in the proposed driver, the average of the input current is kept constant while the peak of the pulsating input current - which passes from the switch and freewheeling diode - is decreased. Moreover, power losses of the semiconductor components in the proposed driver are investigated, and consequently decreased, leading to improvement in the system's overall efficiency. Finally, a 10 W experimental driver is built and tested. The experimental results are consistent with theoretical analysis.

Keywords — Buck converter; High-efficient LED driver; Single stage driver; Integrated converters; Power losses.

1. INTRODUCTION

Today, light-emitting-diodes (LEDs) are widely known due to their significant advantages. They present different features like high efficiency of output light intensity over input electrical power, long life span, small size, robustness, and high reliability. They also have environmentally friendly characteristics rather than fluorescent lamps and are five times more efficient than incandescent lamps. LEDs cannot be connected directly to the grid. A LED driver is needed to use LEDs as a lighting lamp [1-4]. Generally, two power-conversion stages exist in LED drivers: the first one is a power factor correction (PFC) stage, and the second one is a DC/DC stage. The PFC stage is used to comply with IEC61000 3-2 class C regulations. It is used to achieve high power factor and low total harmonic distortion (THD) in the sending end and the latter provides current or voltage regulations for the LEDs in the receiving end. Usually, PWM converters such as buck, boost, buck-boost, SEPIC, and flyback converters are used in LED drivers to play the role of PFC and DC/DC stages. These converters have a simple circuit structure and can be controlled in an easy way [5–11]. Two-stage drivers are designed and optimized efficiently but more circuit components are used, and their total cost is high. Also, due to additional power losses of switches, the system efficiency is decreased while loss analysis and efficiency improvements are counted as the

primary concern of researchers, in recent years [12]. So, to avoid these disadvantages, single-stage LED drivers are widely studied. They show many advantages like lower cost, faster dynamic response, and higher efficiency than two-single drivers. Despite their benefits, high voltage stress would be imposed on MOSFETs in some of the single-stage drivers. This forces designers to use the higher voltage rating MOSFETs, which causes reduced efficiency due to the consequent large $R_{ds,on}$. Also, size and cost are increased consequently [13, 14]. From the switching point of view, converters can be divided into two groups: PWM and resonant converters. In a resonant converter, a resonant circuit is added to the PWM converter to achieve soft-switching characteristics. Hard switching is a serious drawback in the PWM converters. It happens when an active switch is turned on or off and causes high current or voltage spikes. These increase switching losses and decrease efficiency and system reliability, while efficiency is a key factor of design in low-power applications [15- 19]. An LLC converter is widely used in high-power systems because of its high efficiency [20, 21], but LLC shows a higher cost than a single switch converter in medium and low-power applications [22]. On the other hand, to improve the hard-switching effect, the active clamp circuit or the snubber circuit usually are used in the PWM converters [23, 24]. These technologies can provide soft-switching conditions on the active switch to operate at zero voltage switching (ZVS) or zero current switching (ZCS) and help the voltage or current stresses to be reduced. In which, the switching losses are reduced but, there is another problem. These technologies require additional auxiliary switches, diodes, and passive components, which causes the circuit cost to be increased. Additionally, the conduction losses of the active clamp or snubber circuits avoid improving efficiency [25, 26]. One of the most popular topologies for LED drivers is the buck converter. It has a simple structure and a simple control method. Also, the low voltage stress of the switch, which is limited to the input voltage, provides high efficiency. Besides these good features, a large dead angle, which negatively affects PF and current harmonics, is counted as a big problem of the PF corrector buck converter. Dead angle is the angle where the input voltage is lower than the output voltage and the input current does not flow. So, low output voltages are preferred to provide a smaller dead angle and higher PF, but low output voltage harms the circuit efficiency improvement [27]. In [27], a single-stage LED driver based on buck topology, which has current path control switches, is proposed. Using this structure, the LED string can be scalable, and the output voltage becomes adjustable, which helps the dead angle to be reduced, and the efficiency is very high. In [28], a ZVS quasi-resonant inverted buck converter is used as an LED driver. Switching loss is eliminated by ZVS through the parasitic drain capacitance which leads to high power efficiency. A high-efficiency Quasi-resonant Buck driver is studied and designed in [29]. The ZVS condition is guaranteed using a simple inductor zero current detector method and an RC delay circuit. In [30], a hybrid switched-inductor buck converter is utilized as a PFC to implement a high-efficiency LED driver. The topology has lower losses compared to conventional buck topology and is suitable for universal input range. A two-input floating buck-based LED driver is proposed in [31]. Using this structure, the voltage stress is decreased, and high-power efficiency is achieved consequently. Also, a variable off-time control is proposed to adjust the off-time period considering the number of series LEDs and input voltage. Series resonant converter (SRC) based LED driver is proposed in [32]. SRC topology can provide high efficiency for a wide

range of output power. A LED driver is proposed in [33] based on a CLCL resonant converter. It uses two buck-boost circuits as a PFC stage and CLCL resonant converter to provide soft-switching characteristics and high efficiency. Due to the buck-boost input characteristic, it has a near unity power factor and low THD. In [34], the losses of an integrated buck-flyback LED driver are analyzed to improve efficiency. It is shown that the obtained equations help improve the efficiency by changing the parameter values like turn ratio, magnetizing inductance, buck inductance, and bulk capacitor. In this paper, a novel single-stage LED driver based on the buck is proposed. The driver structure is made by combining the buck and buck-boost converters. In the proposed driver efficiency is improved without using any active clamp or snubber circuit. The LED arrangement in the conventional buck driver can be changed using the proposed driver, while the power of the system and switching frequency are kept constant, and the system efficiency is improved by changing the inductor size, switch peak current, and duty ratio.

In summary, the main contributions of this paper are as follows:
- Efficiency improvement is performed without using any snubber circuit.
- The peak pulse current of the switch declines while the power of the driver is kept constant.

The rest of the paper is organized as follows: In section 2, the system configuration and principle of rearranging the LEDs are described in detail. The effect of LEDs rearrangement on the power losses of different components of the proposed driver is investigated in section 3. Section 4 describes the implementation of the proposed LED driver and presents experimental results and finally conclusions are given in section 5.

2.   THE PROPOSED LED DRIVER

This section discusses the circuit configuration and operation principles of the proposed driver.

2.1. Circuit Configuration

Considering the voltage and current characteristics of the power MOSFET with an inductive load, shown in Fig. 1(a) the origin of switch turn-on-turn-off losses is known. The formula used to estimate the switching losses is:

$$P_{SW} = \frac{1}{2} V_D I_D \left(t_{on} + t_{off} \right) + \frac{1}{2} C_{oss} V_D^2 f \tag{1}$$

where f is switching frequency, t_{on}, and t_{off} are MOSFET turn-on and turn-off intervals and C_{oss} shows parasitic capacitances of the switch. Considering Eq. (1) decreasing I_D, V_D and f causes the switching losses to be decreased. In a power circuit, V_D is imposed by the network but I_D and f are the design factors. So, the switching losses can be controlled by controlling the values of I_D and f.

Considering Eq. (1) frequency increment causes the losses to be increased. Although decreasing the frequency helps to efficiency improvement on the other hand causes the size of the circuit inductors and capacitors to become larger and negatively affects the size of the driver, this research concentrates on controlling I_D for efficiency improvement. The effect of increasing the I_D on the turn-on power loss of the switch is shown in Fig.1(b).

The effect of I_D on the turn-off power loss of the switch while MOSFET turns off is the same as turning on.

Here the relations of I_D, $P_{SW}(t)$, and f are considered and a new LED driver that helps to improve the LED driver efficiency is proposed. Fig. 2 shows the proposed driver. In Fig. 2(a) shows the start point of combining buck and buck-boost converters which is simplified and shown in Fig. 2(b).

In the proposed topology, L_{Buck} and $L_{Buckboost}$ are unified and considered as the single inductor L, and also, D_{Buck} and $D_{Buckboost}$ are unified as D. In the proposed driver, rather than typical buck driver, LEDs are divided into two group switches, which helps us to control the input current and subsequently helps to improve the driver efficiency. The detail of LEDs re-arrangement and the operation principle of the proposed driver is represented in part B.
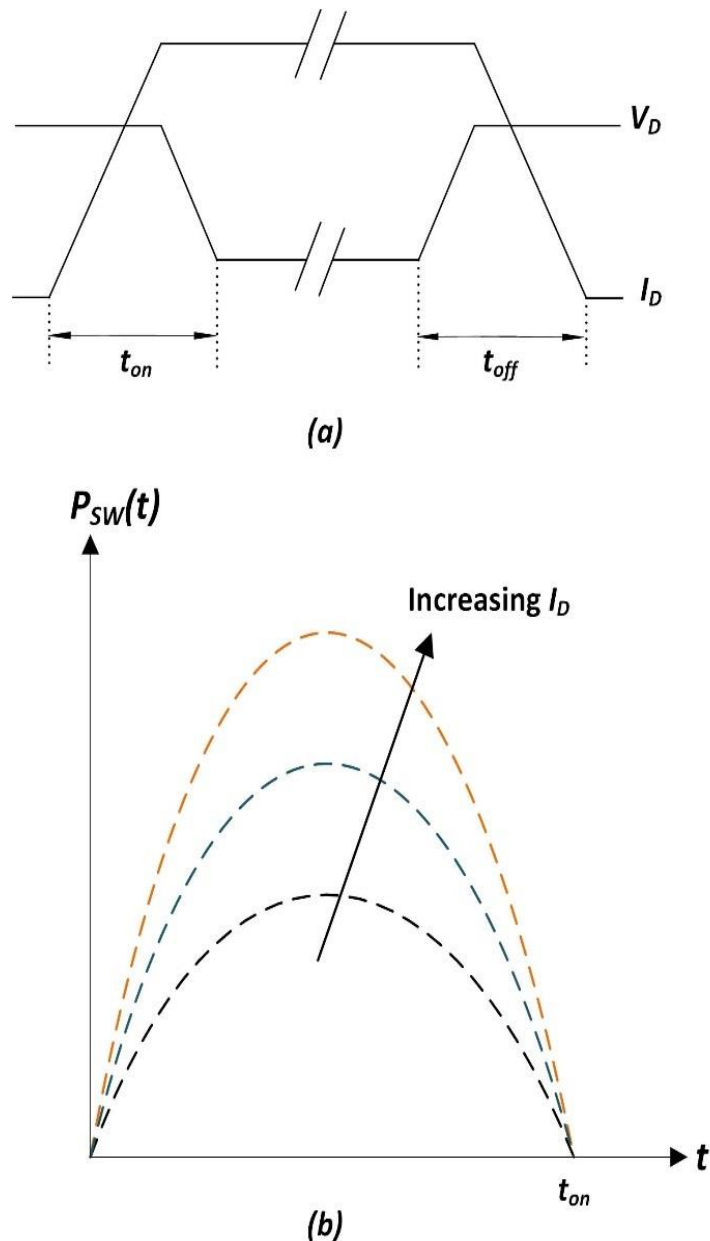

Fig. 1. a) The switched voltage and current of the MOSFET; b) the effect of increasing I_D on the turn-on power loss of the switch.
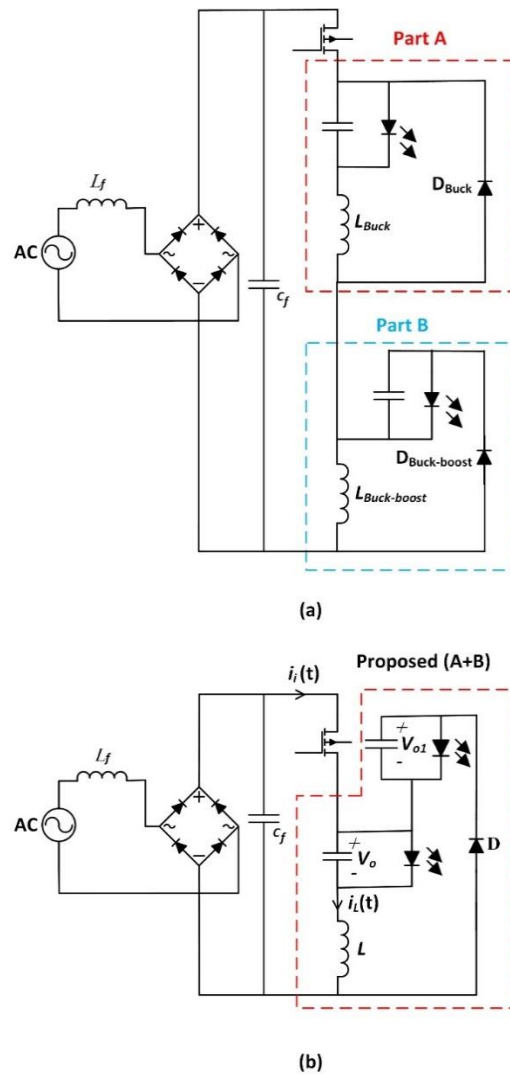
Fig. 2. The driver creating method: a) buck and buck-boost topology; b) the proposed topology.

2.2.   Operation Principle

In this paper, the goal is to improve the efficiency of a predesigned buck LED driver using the proposed driver by decreasing the current flows through the MOSFET while the system power and switching frequency are kept constant. So, the first aim concentrates on the power and switching frequency. Considering the average current in the front end we have:

$$\bar{i}_{i\text{-}buck}(t) \propto \frac{D_{buck}^2 T_{buck}}{L_{buck}} \tag{2}$$

where $i_{i\text{-}buck}(t)$ is the pulsating input current, $i_{i\text{-}buck}(t)$ represents the average of $i_{i\text{-}buck}(t)$, L_{buck} is the inductance of the buck driver, and D_{buck} and T_{buck} are duty ratio and switching period respectively. Regarding the inductor current waveform shown in Fig. 3 we will have:

$$D_{buck} = \frac{T_{1\text{-}buck}}{T_{buck}} \tag{3}$$

Using Eq. (3), Eq. (2) is rewritten by Eq. (4).

$$\bar{i}_{i\text{-}buck}(t) \propto \frac{T_{1\text{-}buck}^2}{L_{buk} T_{buck}} \tag{4}$$

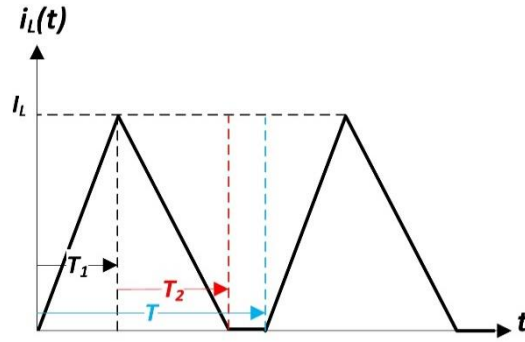where $T_{1\text{-}buck}$ is the period when the switch is turned on (and the inductor is being charged).

Fig. 3. Inductor current waveform.

According to the current ramp equation the peak value of $i_{i\text{-}buck}(t)$ is calculated by Eq. (5):

$$i_{i\text{-}buck\text{-}peak} = \frac{(V_p\text{-}V_o)T_{1\text{-}buck}}{L_{buck}}$$

(5)

where V_p is the peak of the input voltage and V_o shows the output voltage. Due to power factor and efficiency-related issues, it is assumed that V_o is not increased or decreased after LEDs rearrangement. So, to keep the driver input power constant, $i_{i\text{-}buck}(t)$ must be kept constant and according to Eq. (5), $T_{1\text{-}buck}$ and L_{buck} can be used to reach the goal. Regarding Eq. (1), increasing f (which equals to decreasing $T_{1\text{-}buck}$) negatively affects MOSFET power losses and decreasing f causes the input filter to become larger. Thus, the switching frequency should be kept constant. As mentioned before, decreasing I_D causes the MOSFET power losses to be decreased. So, the variables must be changed in a way that satisfies the cited terms. According to Eq. (5), increasing L_{buck} causes the $i_{i\text{-}buck\text{-}peak}$ to be decreased. Hence increasing L_{buck} is counted as the start point of the designing process and is defined as following:

$$L = aL_{buck} \quad a>1$$

(6)

where a is the incremental coefficient of the buck inductor. To keep the power of the driver constant we will have:

$$\bar{i}_i(t) = \bar{i}_{i\text{-}buck}(t)$$

(7)

where $i_i(t)$ is the average pulsating input current of the proposed driver. Using Eqs. (4) and (7) we will give:

$$i_i(t) = \frac{1}{\sqrt{a}} i_{i\text{-}buck}(t)$$

(8)

Eq. (8) shows that the peak current passed through the MOSFET in the proposed driver is decreased rather than the buck driver. The next step is to complete the designing process while the switching frequency and power of the driver are kept constant. It is supposed that the buck driver works in boundary mode while the input voltage has its maximum value. In boundary mode, the switching period is calculated by:

$$T_{buck} = T_{1\text{-}buck} + T_{2\text{-}buck}$$

(9)

While the input voltage has its maximum value (the boundary mode) $T_{2\text{-}buck}$ is the time that is required to discharge the inductor. Definitely, at other switching periods, since I_L is less than $I_{L\text{-}peak}$ the inductor is discharged during the $T_{2\text{-}buck}$ calculated for boundary mode. In the proposed driver the voltage that causes the inductor to be discharged is calculated by:

$$V_{o2} = V_{o1} + V_o$$

(10)

where V_{o2} is the voltage that discharges the inductor of the proposed driver. V_{o1} helps to keep the frequency constant and subsequently helps to improve efficiency. According to this, $T=T_{buck}$ and we will have:

$$T_2 = \frac{\sqrt{a}I_{L\text{-}peak}L_{buck}}{V_{o1}+V_o}$$

(11)

Here V_{in} is defined by:

$$V_{in} = V_p - V_o$$

(12)

Using Eqs. (10) - to (12) we will give:

$$V_{o2\text{-}min} = \frac{\sqrt{a}V_{in}V_o}{V_{in}+V_o(1-\sqrt{a})}$$

(13)

Using Eq. (13) the minimum voltage ($V_{o2\text{-}min}$) that is required to stay in boundary mode and keep the frequency constant is calculated. According to the calculated V_{o2} and the LEDs nominal current, LEDs rearrangement in part B is performed. Regarding the new LEDs arrangement, the current of the new branch(es) must be calculated to remain in the LEDs nominal current range. To calculate V_{o2}, a must be calculated first. Suppose the load of a predesigned buck LED driver is shown in Fig. 4.
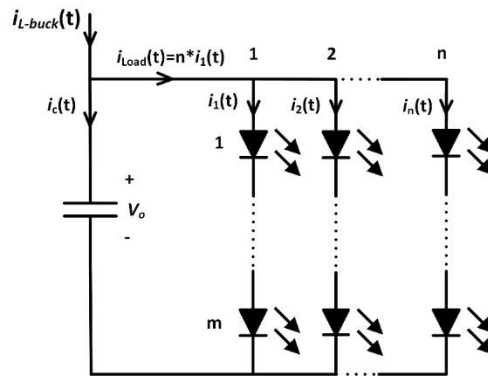

Fig. 4. The load of a predesigned buck LED driver.

The load contains m ∗ n LEDs where m shows the number of series LEDs and n shows the number of parallel branches. For simplification it is supposed that $i_1(t) = i_2(t) = \cdots = i_n(t)$. By calculating the average value of $i_{L\text{-}buck}(t)$ in the T interval, we will give:

$$i_{Load}(t) = n.i_1(t) = \bar{i}_{L\text{-}buck}(t)$$

(14)

The waveforms of $i_{L\text{-}buck}(t)$ and $i_{Load}(t)$ are shown in Fig. 5.
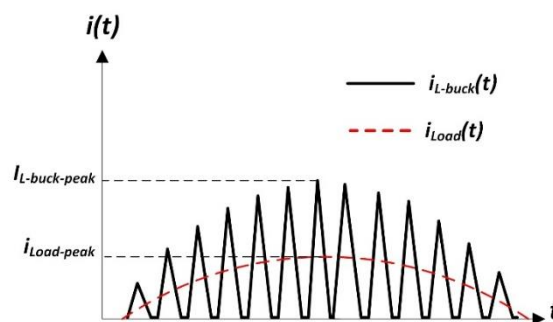

Fig. 5. Waveforms of $i_{L\text{-}buck}(t)$ and $i_{Load}(t)$.

As mentioned before, regarding that we want to keep the dead angle constant, a design process is based on the number of branches n (this means that V_o is kept constant). It should

be noted that the peak of i_1 must not exceed the LEDs nominal current. Here we have:

$$i_{Load-peak} = \frac{1}{2}I_{L-buck-peak}$$ (15)

According to Fig. 5 and Eq. (15), the current passed through the LEDs has its maximum value for $I_{L-buck-peak}$. Suppose that x branches are picked out to move from part A (buck) to B (buck-boost). According to this, we will get:

$$\frac{1}{2}I_{L-peak} = (n-x)i_{Load-peak}$$ (16)

where I_{L-peak} is the maximum inductor current of the proposed driver. Considering Eqs. (15) and (16):

$$I_{L-peak} = \frac{n-x}{n}I_{L-buck-peak}$$ (17)

Using Eqs. (8) and (17) we will give:

$$\sqrt{a} = \frac{n}{n-x}$$ (18)

According to Eq. (18), a larger x leads to a larger a. According to Eqs. (1) and (8), a larger a leads to a smaller $i_i(t)$ and P_{SW}. So, increasing a causes the switching losses to be decreased. The effect of increasing a on the other parts of the proposed driver is investigated in section 3. As mentioned before, after calculating V_{o2}, the current passed through the LEDs must be calculated to ensure that it doesn't exceed the LEDs nominal current. Also, according to Eq. (15), the maximum current passed through the LEDs corresponds to I_{L-peak}. So, the current must be calculated in the interval where I_{L-peak} occurs. In this interval, the driver works in boundary mode. This is explained in detail according to Fig. 4. The current of different parts of the load are defined and shown in Fig. 6.
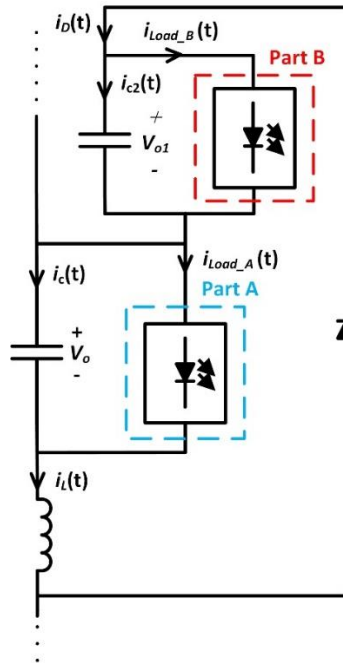

Fig. 6. Load arrangement of the proposed driver.

According to Fig. 6, $i_{Load-A}(t) = i_L(t)$ is passed through part A and $i_{Load-B}(t) = i_D(t)$ is passed through part B. The topological stages of the proposed driver in the interval where I_{L-peak} occurs is shown in Fig. 7.
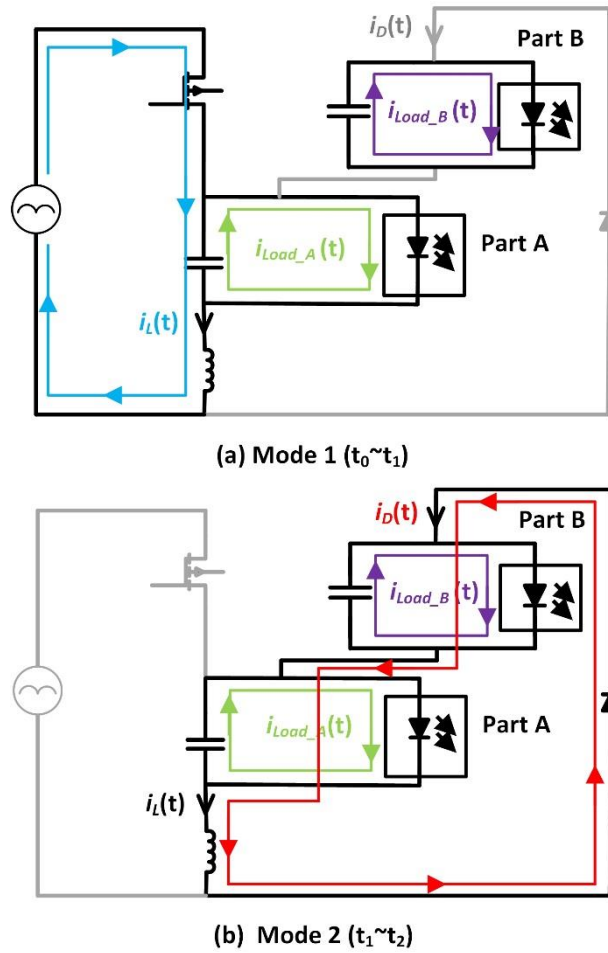
(a) Mode 1 (t₀~t₁)

(b) Mode 2 (t₁~t₂)

Fig. 7. Topological stages of the proposed driver in the interval where $I_{L\text{-}peak}$ occurs while the switch is turned: a) on; b) off.

Considering Fig. 7, the waveforms of $i_L(t)$, $i_{Load\text{-}A}(t)$, $i_D(t)$ and $i_{Load\text{-}B}(t)$ are shown in Fig. 8.
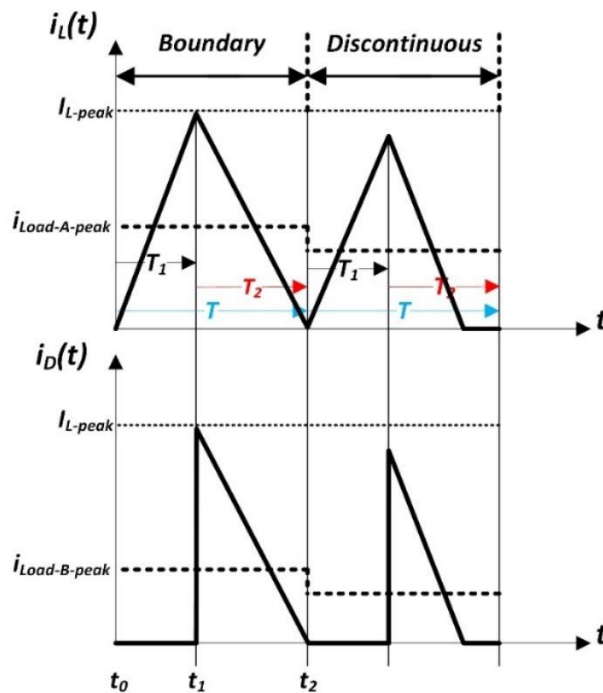

Fig. 8. The waveforms of $i_L(t)$, $i_{Load\text{-}A}(t)$, $i_D(t)$ and $i_{Load\text{-}B}(t)$.

Since the maximum value of $i_{Load-B}(t)$ occurs during $t_0 \sim t_2$ (when boundary mode happens), this interval is considered to calculate the current sharing between part A and B. In this way we will have:

$$\frac{i_{Load-B-peak}}{i_{Load-A-peak}} = \frac{T_2}{T_1+T_2} \tag{19}$$

LEDs arrangement in part B is performed based on V_{o2} and $i_{Load-B-peak}$. The calculated current in part B should remain in the LEDs nominal current range otherwise, it is required to change the LEDs arrangement in part B. On the other hand, using Eq. (19) the current of LEDs in part B is controlled indirectly in a way that it does not exceed the LEDs nominal current. The LEDs arrangement in part B is achieved by the following procedure:

1) The number of series LEDs (m_b) is calculated by:

$$m_b = (V_{o2-min} - V_o)/V_f \tag{20}$$

where, V_f shows the LED forward voltage. It should be noted that m_b is rounded to the nearest higher value to ensure that V_{o2-min} is guaranteed. Real value of V_{o2} is calculated using the following equation:

$$V_{o2} = m_b V_f + V_o \tag{21}$$

2) The number of parallel branches (n_b) is calculated by:

$$n_b = (i_{Load-B-peak})/I_f \tag{22}$$

where, I_f presents the LED forward (nominal) current and n_b is rounded to the nearest higher value to ensure that the current doesn't exceed the LEDs nominal current in part B. T_2 is achieved by:

$$T_2 = (LI_{L-peak})/V_{o2} \tag{23}$$

3.   POWER LOSSES OF DIFFERENT COMPONENTS OF THE PROPOSED DRIVER

In this section, the effect of LEDs rearrangement on the power losses of the freewheeling diode and switch are investigated.

3.1.   Losses of the Freewheeling Diode

The freewheeling diode D is considered first. Since working in critical mode, the diode is soft switched while it turns off and its loss is neglected. So, the turn-on and conducting losses are investigated. For a better comparison between diode conduction losses in the conventional buck driver and the proposed driver, the diode current waveforms of both drivers are shown in Fig. 9 in a single switching period.
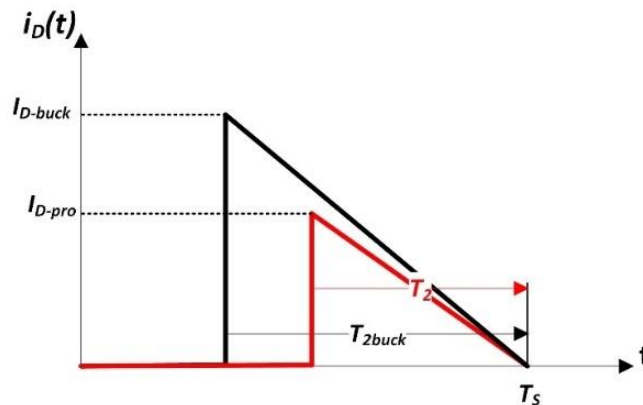

Fig. 9. The diode current waveforms of the buck and the proposed drivers in a single switching period.

Conduction loss is calculated using the following equation:

$$P_{loss} = \frac{1}{T_s} \int V_D(t) I_D(t) dt \tag{24}$$

where, P_{loss} shows the diode conduction loss in a single switching period and $V_D(t)$ and $I_D(t)$ represent the voltage and current of the diode respectively. Considering that $V_D(t)$ is almost constant we get:

$$\frac{P_{loss-pro}}{P_{loss-buck}} = \frac{\int I_{D-pro}(t) dt}{\int I_{D-buck}(t) dt} = \frac{T_2 I_{D-pro}}{T_{2-buck} I_{D-buck}} \tag{25}$$

Considering $T_2 < T_{2-buck}$ and $I_{D-pro} < I_{D-buck}$ we have $P_{loss-pro} < P_{loss-buck}$ which means that the diode conduction loss in the proposed driver is less than the conventional buck driver. It can be shown that diode turn-on losses of both drivers are related as follows:

$$\frac{P_{turn-off-pro}}{P_{turn-off-buck}} = \frac{1}{\sqrt{a}} \left(1 + \frac{V_{o1}}{V_p} \frac{\int_{\theta_d}^{\frac{\pi}{2}} (V_p \sin\theta - V_o) d\theta}{\int_{\theta_d}^{\frac{\pi}{2}} \sin\theta (V_p \sin\theta - V_o) d\theta} \right) \tag{26}$$

According to the design parameters, it can be shown that Eq. (26) is less than 1. Similar results can be achieved for switch turn-off losses.

3.2. Switch Losses

Due to working in critical mode, the switch is soft-switched while it turns on and the loss is neglected. As mentioned before, according to Eq. (26) the switch turn-off loss for the proposed driver is less than the conventional buck driver. To compare the conducting loss, switch current waveforms of the proposed and conventional buck drivers are shown in Fig. 10.
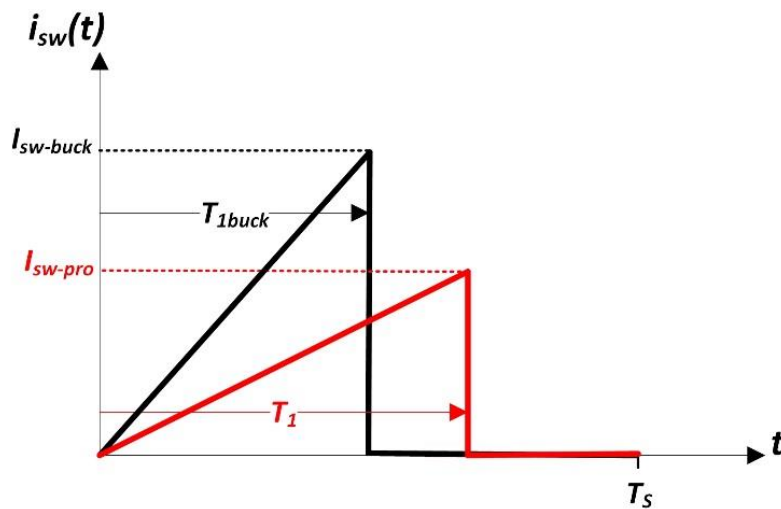

Fig. 10. The switch current waveforms of buck and the proposed drivers in a single switching period

It can be shown that:

$$\frac{P_{loss-sw-pro}}{P_{loss-sw-buck}} = \frac{\int I_{sw-pro}^2(t) dt}{\int I_{sw-buck}^2(t) dt} = \frac{T_1 I_{sw-pro}^2}{T_{1-buck} I_{sw-buck}^2} \tag{27}$$

where $P_{loss-sw-pro}$ shows the switch conducting loss of the proposed driver and $P_{loss-sw-buck}$ relates to the conventional buck driver. Using Eq. (27) we will have:

$$\frac{P_{loss-sw-pro}}{P_{loss-sw-buck}} = \frac{\sqrt{a} T_{1-buck} \frac{I_{sw-buck}^2}{a}}{T_{1-buck} I_{sw-buck}^2} = \frac{1}{\sqrt{a}} < 1 \tag{28}$$

Regarding Eq. (28), the conducting loss of the switch of the proposed driver is less than conventional buck driver. According to the results, total losses of switch and diode in the proposed driver are less than the conventional buck driver.

4.   EXPERIMENTAL RESULTS

In order to verify the performance of the proposed driver, a driver setup is made up and tested. The setup implementation of the proposed driver is shown in Fig. 11. A 10w buck-based LED driver with 40 LEDs (m=10, n=4) is considered and then the proposed driver is designed based on it. To show the performance of the proposed driver the efficiency of both drivers is compared. LEDs arrangement consists of 4 parallel branches of 10 series LEDs. Switching frequency and buck inductor size are chosen to be 40Khz and 500uH respectively. The flowchart of design procedure of the proposed driver is shown in Fig. 12 and designed parameters of the conventional and proposed drivers are shown in Table 1 and 2 respectively.
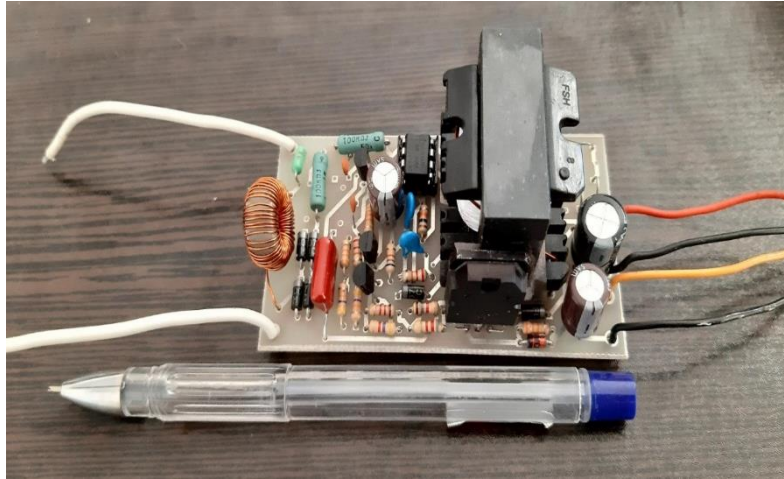

Fig. 11. Setup of the proposed driver.

Table 1. Design parameters of the conventional buck driver.

| Symbol	Description	Value
V_{IN}	Input AC line voltage	110 V_{rms}
V_p	Peak of the input voltage	155.6 V
V_{in}	The voltage defined in Eq. (12)	122.1 V
V_f	LED forward voltage	3.35 V
I_f	LED nominal current	150 mA
N	Number of LEDs	40
m	Number of series LEDs each branch in part A	10
n	Number of parallel branches in part A	4
V_o	Output voltage in part A	33.5 V
L_{buck}	Inductance of the conventional buck driver	500 μH
I_{L-peak}	MOSFET drain-source peak current	1200 mA
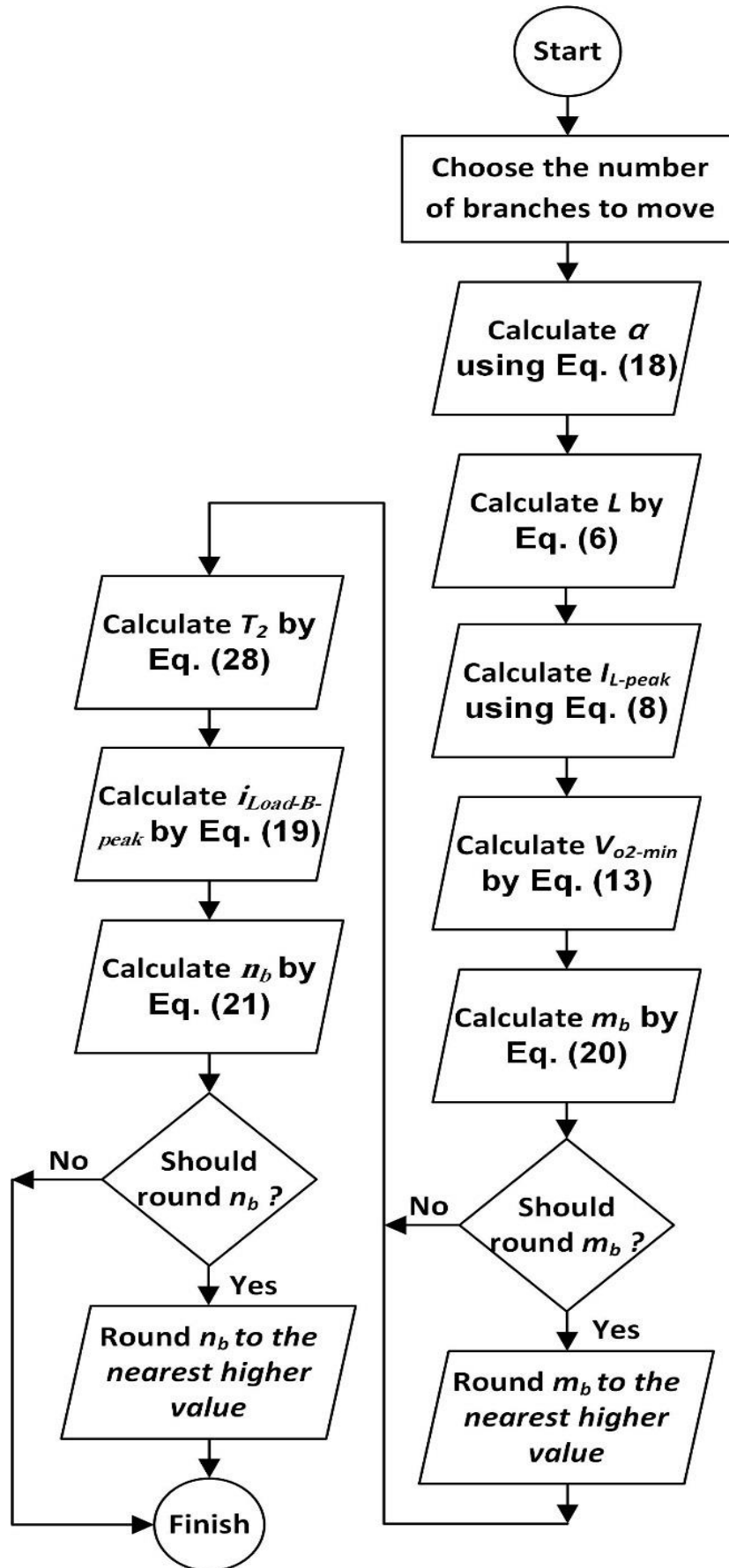
Fig. 12. Flowchart of the proposed driver design procedure.

Regarding Table 2, for $x=3$ The required minimum output voltage to stay in boundary mode has a very large value that corresponds to a large number of LEDs. So, this condition is not examined. For $x=2$, the value of $i_{Load\text{-}B\text{-}peak}$ is very close to the LEDs nominal current and therefore n_b is not rounded to the nearest higher value. To compare the practical and theoretical waveforms of $i_{SW}(t)$ and $i_D(t)$, the inductor current is considered. Fig. 13 shows the measured waveforms of inductor current i_L and gate voltage V_g for the proposed driver for $x=1, 2$.

Table 2. Design parameters of the proposed driver.

Symbol	Value		
	x = 1	x = 2	x = 3
a	1.78	4	16
L	890 μH	2 mH	8 mH
I_{Lpeak}	900 mA	600 mA	300 mA
$i_{Load\text{-}A\text{-}peak}$	450 mA	300 mA	-
$i_{Load\text{-}B\text{-}peak}$	287 mA	153.48 mA	-
$V_{o2\text{-}min}$	49.2 V	92.33 V	757.47 V
V_{o2}	50.25 V	93.8 V	-
T_2	15.94 μS	12.79 μS	-
m	10	10	-
n	3	2	-
mb	5	18	-
nb	2	1	-
N	40	38	-
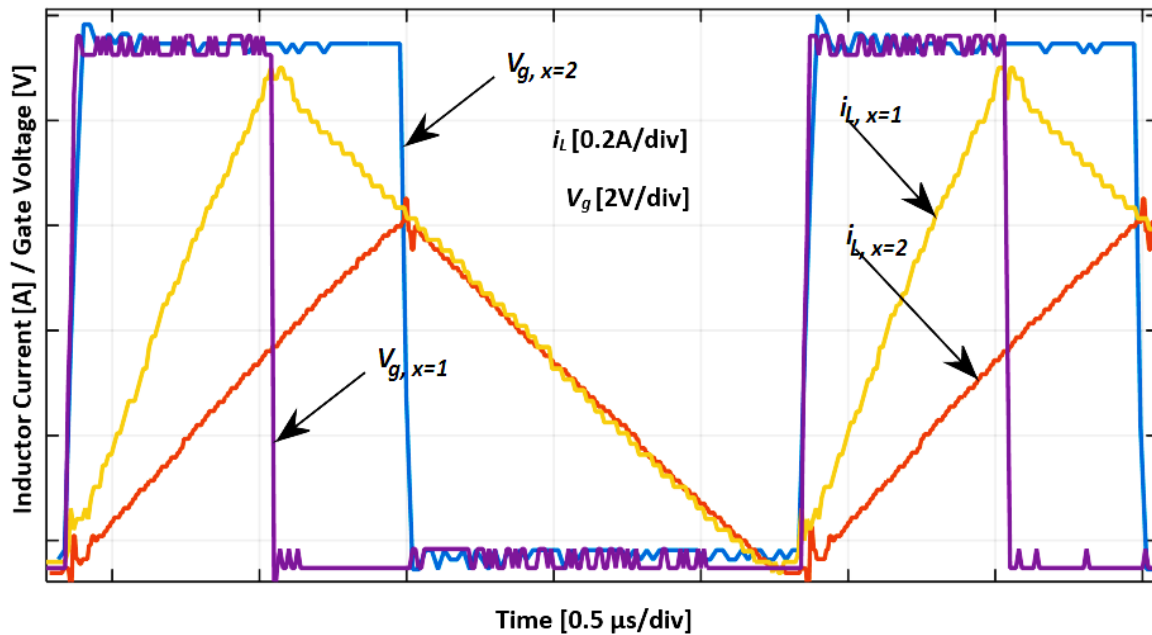
Fig. 13. Waveforms of the inductor current and gate voltage in the proposed driver for $x = 1, 2$.

The waveforms of the proposed driver show that the measured waveforms are in agreement with the theoretical waveforms shown in Fig. 9. The waveforms of output voltages of the proposed driver for x=1, 2, and also, the input voltage and current are shown in Fig. 14.
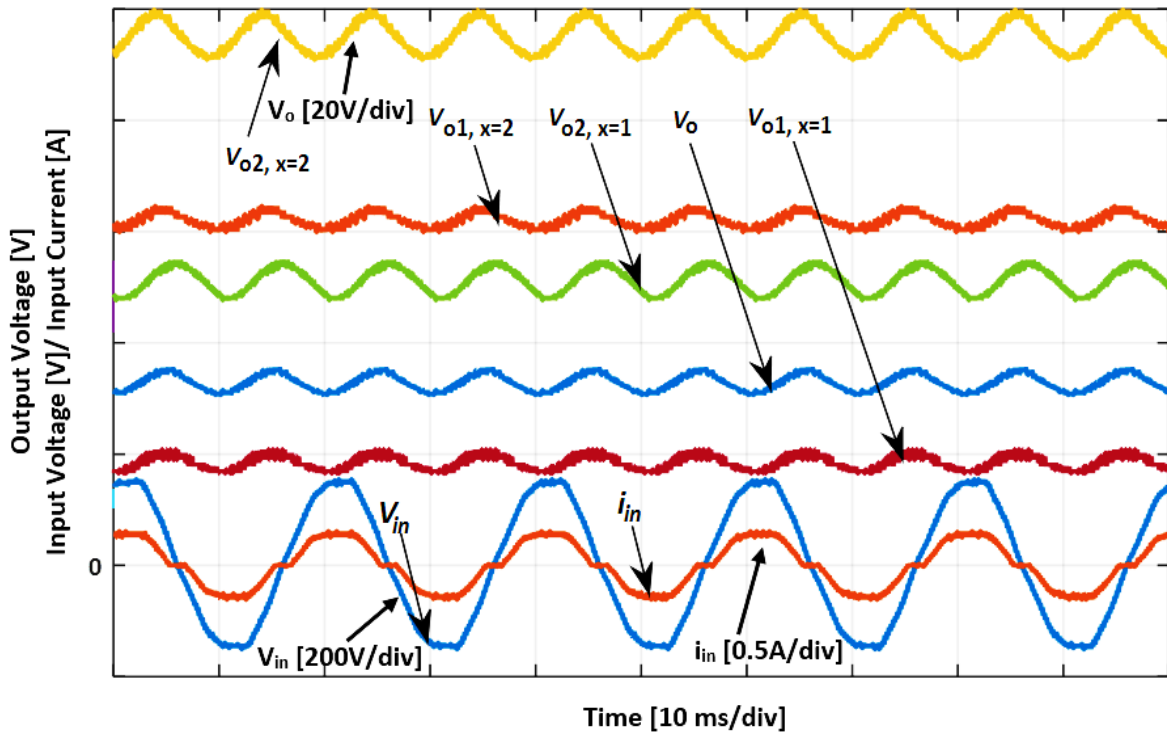

Fig. 14. Waveforms of different output voltages of the proposed driver for x = 1, 2 and input voltage and current.

It is seen that the output voltages comply with data presented in Table 2. The output currents (i_{load-A} and i_{load-B}) are shown in Fig. 15 for x=2, which correspond to the achieved data in Table 2.
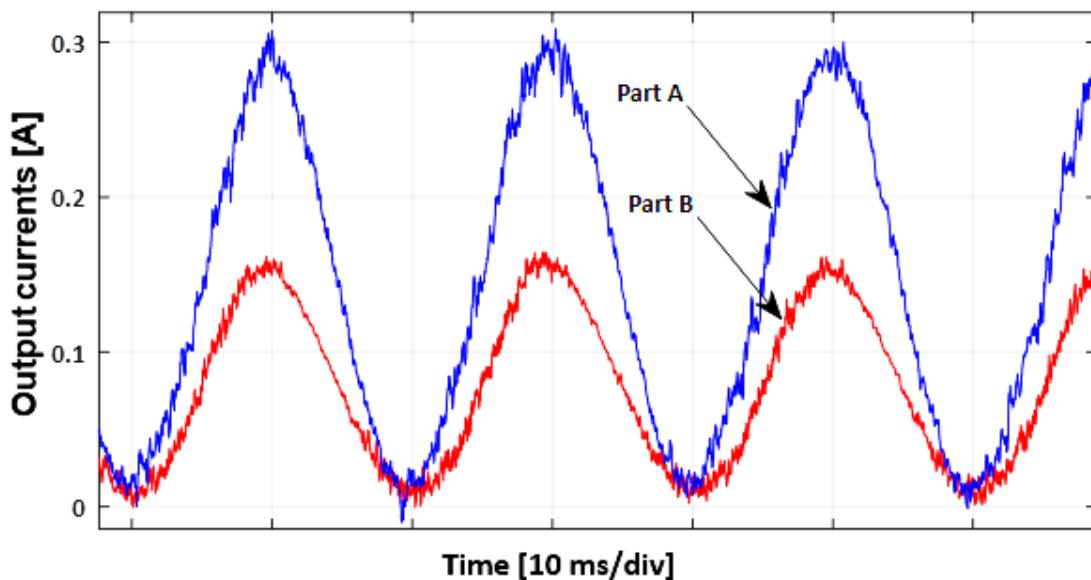

Fig. 15. Waveforms of output currents for x = 2 in parts A and B.

Fig. 16 shows the efficiency of the proposed and conventional drivers as a function of the peak of the pulsating input current and the corresponding x.
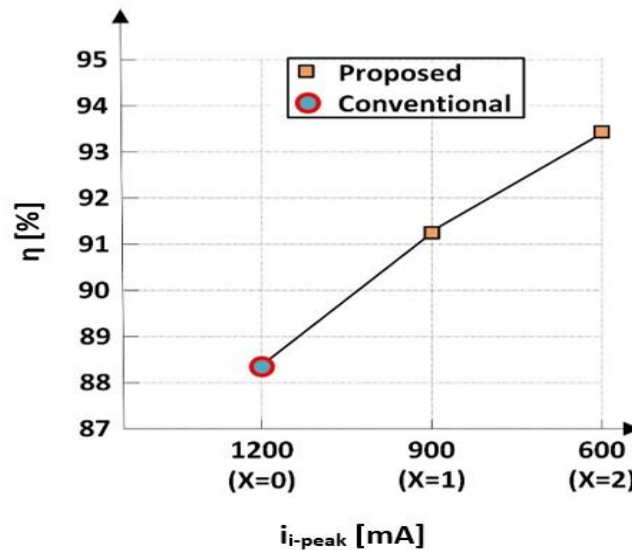
Fig. 16. The efficiency of the proposed (x = 1, 2) and the conventional driver(x = 0).

It is seen that as x increases, the losses of the proposed driver become smaller. Fig. 17 shows the harmonic spectrum of the input current in comparison with IEC61000-3-2 limits. As it is seen the current harmonics comply with the standard limits for each harmonic order.
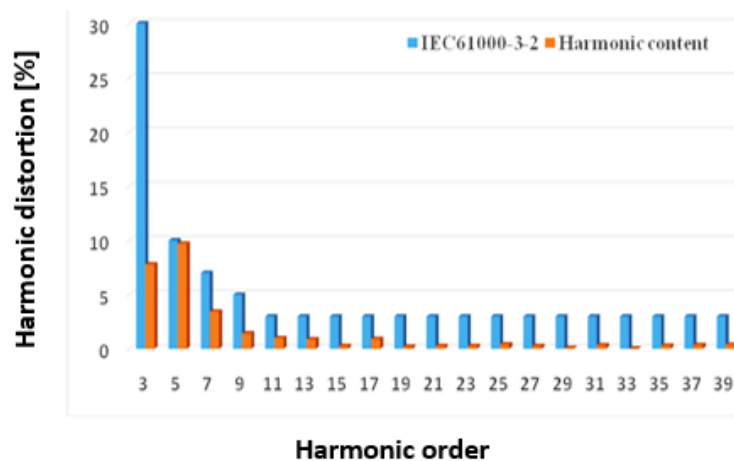

Fig. 17. The input current harmonic contents.

As seen, the efficiency of the conventional buck is lower than the proposed driver for the range of x. In addition, at a higher range of x, the efficiency difference between two drivers is more. The maximum efficiency of the proposed driver reaches 93.3% for x=2 while the efficiency of the conventional buck driver is 88.3%. The number of diodes, MOSFETs and inductors of both drivers are the same and both drivers show equal THD and power factor values. The proposed driver only has a more capacitor used as output capacitor after the load rearrangement. The proposed driver is compared with some similar research in Table 3. As seen, the proposed driver with no THD regulations requires one MOSFET, one magnetic core, one diode, and three capacitors while the previous research requires more devices and with THD regulations only one more inductor is needed. Furthermore, high-efficiency, high power factor and low THD are achieved without increasing the hardware and controller complexity. Besides proposing structures, for the efficiency improvement, [35, 39] use digital control and valley switching method is used in [36] while the proposed driver is simply

controlled by a single switching pulse with constant duty cycle and frequency. [37] uses a passive snubber circuit and the number of elements used in [38] is comparable to the proposed driver.

Table 3. Comparison of the proposed driver with similar - reported in literature - ones.

Ref.	MOSFET	Capacitor	Magnetic core	Diode	Input ac RMS voltage	Power factor	THD (%)	Output power	η (%)
[35]	1	2	1 inductor	4	110-120	0.994	10	26.5	92.61
[36]	1	3	1 coupled inductor	2	220	/	/	15	97
[37]	1	4	2 inductors	3	24 VDC	/	/	15	92
[38]	2	4	3 inductors	2	220	0.98	9	30	89.5
[39]	4	12	1 inductor + 2 transformers	8	230	/	/	15	93
This work	1	3	2 inductors with THD regulations	1	110	0.988	15.4	10	x=1 91.2
			1 inductor without THD regulations						x=2 93.3

5.   CONCLUSIONS

This paper proposed a novel 110 V_{rms} ac-dc LED driver that helps improve efficiency without using any active or passive components. The circuit configuration was obtained by combining buck and buck-boost converters. The proposed single stage single switch driver uses only one freewheeling diode and one inductor. The feasibility of the proposed driver was validated by experimental results. Changing the load arrangement helped to increase the output voltage, decrease the inductor discharge period, increase the size of the inductor, and decrease the peak of the current passing through the switched components while the working frequency is kept constant. The peak current reduction with a constant switching frequency helped to reduce the switching losses of switch and freewheeling diode. Also, by the peak current reduction and changing the inductor charge and discharge periods during a constant frequency the average current passing through the freewheeling diode and switch was reduced and helped to decrease the conduction losses. Along with the simple structure, the driver presented a good feature of high efficiency. At the rated power the efficiency was 93.3%.

REFERENCES

[1]   H. Ahn, S. Hong, O. Kwon, "A highly accurate current LED lamp driver with removal of low-frequency flicker using average current control method," *IEEE Transactions on Power Electronics*, vol. 33, no. 10, pp. 8741–8753, 2018, doi: 10.1109/TPEL.2017.2783921.

[2] M. Mahmoud, "Indoor-lighting system design using simultaneous control of LEDs lighting intensity and roller blinds' opening for economic energy consumption," *Jordan Journal of Electrical Engineering*, vol. 8, no 3, pp. 288-306, 2022, doi:10.5455/jjee.204-1658671735.

[3] D. Do, H. Cha, B. Nguyen, H. Kim, "Two-channel interleaved buck LED driver using current-balancing capacitor," *IEEE Journal of Emerging and Selected Topics in Power Electronics*, vol. 6, no. 3, pp. 1306–1313, 2018, doi: 10.1109/JESTPE.2018.2845858.

[4] C. Cheng, C. Chang, H. Cheng, E. Chang, C. Lai, "A novel LED tube lamp driver with power-factor correction for indoor lighting applications," *IEEE 7th Global Conference on Consumer Electronics (GCCE)*, 2018, doi: 10.1109/GCCE.2018.8574803.

[5] H. Kolla, N. Vishwanathan, B. Murthy, "Independently controllable dual-output half-bridge series resonant converter for LED driver application," *IEEE Journal of Emerging and Selected Topics in Power Electro_nics*, vol. 10, no. 2, pp. 2178–2189, 2022, doi: 10.1109/JESTPE.2021.3120879.

[6] X. Xie, M. Ye, Y. Cai, J. Wu, "An optocouplerless two-stage high power factor LED driver," *Twenty-Sixth Annual IEEE Applied Power Electronics Conference and Exposition (APEC)*, 2011, doi: 10.1109/APEC.2011.5744883.

[7] K. Alawasaa, A. Al-Mbaideen, "Power quality assessment and analysis for low voltage distribution networks," *Jordan Journal of Electrical Engineering*, vol. 4, no 3, pp. 165-175, 2018.

[8] D. Lu, H. H. Iu, V. Pjevalica, "Single-stage AC/DC boost–forward converter with high power factor and regulated bus and output voltages," *IEEE Transactions on Industrial Electronics*, vol. 56, no. 6, pp. 2128–2132, 2009, doi: 10.1109/TIE.2009.2014304.

[9] J. Alonso, J. Vina, D. Vaquero, G. Martinez, R. Osorio, "Analysis and design of the integrated double buck–boost converter as a high-power-factor driver for power-LED lamps," *IEEE Transactions onIndustrial Electronics*, vol. 59, no. 4, pp. 1689–1697, 2012, doi: 10.1109/TIE.2011.2109342.

[10] Y. Wang, Y. Guan, K. Ren, W. Wang, and D. Xu, "A single-stage LED driver based on BCM boost circuit and LLC converter for street lighting system," *IEEE Transactions on Industrial Electronics*, vol. 62, no. 9, pp. 5446–5457, 2015, doi: 10.1109/TIE.2015.2416341.

[11] Y. Wang, Y. Guan, J. Huang, W. Wang, D. Xu, "A single-stage LED driver based on interleaved buck–boost circuit and LLC resonant converter," *IEEE Journal of Emerging and Selected Topics in Power Electronics*, vol. 3, no. 3, pp. 732–741, 2015, doi : 10.1109/JESTPE.2015.2421342.

[12] Y. Wang, J. Alonso, X. Ruan, "A review of LED drivers and related technologies," *IEEE Transactions on Industrial Electronics*, vol. 64, no. 7, pp. 5754–5765, 2017, doi:10.1109/TIE.2017.2677335.

[13] M. Costa, J. Alonso, J. Miranda, J. Garcia, D. Lamar, "A single-stage high-power-factor electronic ballast based on integrated buck flyback converter to supply metal halide lamps," *IEEE Transactions on Industrial Electronics*, vol. 55, no. 3, pp. 1112–1122, 2008, doi: 10.1109/TIE.2007.909729.

[14] C. Cheng, C. Chang, T. Chung, F. Yang, "Design and implementation of a single-stage driver for supplying a LED streetlighting module with power factor corrections," *IEEE Transactions on Power Electronics*, vol. 30, no. 2, pp. 956–966, 2015, doi: 10.1109/TPEL.2014.2312024.

[15] Y. Wang, S. Gao, S. Zhang, D. Xu, "A two-stage quasi-resonant dual-buck LED driver with digital control method," *IEEE Transactions on Industry Applications*, vol. 54, no. 1, pp. 787–795, 2018, doi: 10.1109/IEACON.2016.8067352.

[16] Y. Wang, X. Hu, Y. Guan, D. Xu, "A single-stage LED driver based on half-bridge CLCL resonant converter and buck–boost circuit," *IEEE Journal of Emerging and Selected Topics in Power Electronics*, vol. 7, no. 1, pp. 196–208, 2019, doi: 10.1109/JESTPE.2018.2861740.

[17] H. Wei, I. Batarseh, "Comparison of basic converter topologies for power factor correction," *Proceedings IEEE Southeastcon '98 'Engineering for a New Era'*, Orlando, FL, USA, 1998, doi: 10.1109/SECON.1998.673368.

[18] M. Costa, J. Alonso, J. Miranda, J. Garcia, D. Lamar, "A Single-stage high-power-factor electronic ballast based on integrated buck flyback converter to supply metal halide lamps," *IEEE Transactions on Industrial Electronics*, vol. 55, no. 3, pp. 1112-1122, 2008, doi: 10.1109/TIE.2007.909729.

[19] Y. Xiong, S. Sun, H. Jia, P. Shea, Z. Shen, "New physical insights on power MOSFET switching losses," *IEEE Transactions on Power Electronics*, vol. 24, no. 2, pp. 525-531, 2009, doi: 10.1109/TPEL.2008.2006567.

[20] J. Kim, J. Moon, G. Moon, "Duty-ratio-control-aided LLC converter for current balancing of two-channel led driver," *IEEE Transactions on Industrial Electronics*, vol. 64, no. 2, pp. 1178–1184, 2017, doi: : 10.1109/TIE.2016.2618338..

[21] H. Park, J. Jung, "PWM and PFM hybrid control method for LLC resonant converters in high switching frequency operation," *IEEE Transactions on Industrial Electronics*, vol. 64, no. 1, pp. 253–263, 2017, doi:10.1109/TIE.2016.2599138.

[22] Y. Wang, F. Li, Y. Qiu, S. Gao, Y. Guan, D. Xu, "A single-stage LED driver based on flyback and modified class-e resonant converters with low-voltage stress," *IEEE Transactions on Industrial Electronics*, vol. 66, no. 11, pp. 8463–8473, 2019, doi: 10.1109/TIE.2018.2890502.

[23] J. Lee, D. Yu, J. Kim, Y. Kim, S. Shin, D. Jung, Y. Jung, C. Won, "Auxiliary switch control of a bidirectional softswitching DC/DC converter," *IEEE Transactions on Power Electronics*, vol. 28, no. 12, pp. 5446–5457, 2013, doi: 10.1109/TPEL.2013.2254131.

[24] J. Yun, H. Choe, Y. Hwang, Y. Park, B. Kang, "Improvement of power-conversion efficiency of a DC–DC boost converter using a passive snubber circuit," *IEEE Transactions on Industrial Electronics*, vol. 59, no. 4, pp. 1808–1814, 2012, doi: 10.1109/TIE.2011.2141095.

[25] H. Cheng, Y. Chang, H. Yen, C. Hua, P. Su, "An interleaved flyback-typed LED driver with ZVS and energy recovery of leakage inductance," *IEEE Transactions on Power Electronics*, vol. 34, no. 5, pp. 4497–4508, 2019, doi: 10.1109/TPEL.2018.2864223.

[26] A. Mousavi, P. Das, G. Moschopoulos, "A comparative study of a new ZCS DC–DC full-bridge boost converter with a ZVS active-clamp converter," *IEEE Transactions on Power Electronics*, vol. 27, no. 3, pp. 1347–1358, 2012, doi: 10.1109/TPEL.2011.2118233.

[27] J. Baek, S. Chae, "Single-stage buck-derived LED driver with improved efficiency and power factor using current path control switches," *IEEE Transactions on Industrial Electronics*, vol. 64, no. 10, pp. 7852– 7861, 2017, doi: 10.1109/TIE.2017.2698404.

[28] L. Li, Y. Gao, P. Mok, I. Sun, N. Park, "A 16–28-w 92.8 constant-duty-ratio frequency regulator," *IEEE Transactions on Circuits and Systems II: Express Briefs*, vol. 62, no. 12, pp. 1199–1203, 2015, doi: 10.1109/TCSII.2015.2468925.

[29] J. Wang, F. Zhang, J. Xie, S. Zhang, S. Liu, "Analysis and design of high efficiency quasi-resonant buck converter," *International Power Electronics and Application Conference and Exposition*, pp. 1486–1489, 2014, doi: 10.1109/PEAC.2014.7038084.

[30] Y. Liu, F. Syu, H. Hsieh, K. Kim, H. Chiu, "Hybrid switched-inductor buck PFC converter for high-efficiency LED drivers," *IEEE Transactions on Circuits and Systems II: Express Briefs*, vol. 65, no. 8, pp. 1069–1073, 2018, doi: 10.1109/TCSII.2017.2787554.

[31] P. Liu, R. Lin, H. Chen, "Two-input floating buck converter with variable off-time control scheme for high-efficiency and -accuracy LED lighting," *IEEE Journal of Emerging and Selected Topics in Power Electronics*, vol. 6, no. 2, pp. 563–570, 2018, doi: 10.1109/JESTPE.2017.2788944.

[32] T. Gucin, B. Fincan, M. Bibero, "A series resonant converterbased multichannel LED driver with inherent current balancing and dimming capability," *IEEE Transactions on Power Electronics*, vol. 34, no. 3, pp. 2693–2703, 2019, doi: 10.1109/TPEL.2018.2838261.

[33] Y. Wang, X. Deng, Y. Wang, D. Xu, "Single-stage bridgeless LED driver based on a CLCL resonant converter," *IEEE Transactions on Industry Applications*, vol. 54, no. 2, pp. 1832–1841, 2018, doi: 10.1109/IAS.2017.8101807.

[34] G. Abdelmessih, J. Alonso, M. Costa, "Loss analysis for efficiency improvement of the integrated buck–flyback LED driver," *IEEE Transactions on Industry Applications*, vol. 54, no. 6, pp. 6543– 6553, 2018, doi: 10.1109/IAS.2017.8101801.

[35] G. Abdelmessih, J. Alonso, M. Costa, Y. Chen, W. Tsai, "Fully integrated buck and boost converter as a high efficiency, high-power-density off-line LED driver," *IEEE Transactions on Power Electronics*, vol. 35, no. 11, pp. 12 238–12 251, 2020, doi: 10.1109/TPEL.2020.2993796.

[36] R. Sangrody, M. Pouresmaeil, M. Marzband, E. Pouresmaeil, "Resonance-based optimized buck LED driver using unequal turn ratio coupled inductance," *IEEE Transactions on Power Electronics*, vol. 35, no. 12, pp. 13 068–13 076, 2020, doi: 10.1109/TPEL.2020.2990492.

[37] S. Lee, H. Choe, J. Yun, "Performance improvement of a boost LED driver with high voltage gain for edge-lit LED backlights," *IEEE Transactions on Circuits and Systems II: Express Briefs*, vol. 65, no. 4, pp. 481–485, 2018, doi: 10.1109/TCSII.2017.2716442

[38] Y. Wang, S. Gao, S. Zhang, and D. Xu, "A two-stage quasi-resonant dual-buck LED driver with digital control method," *IEEE Transactions on Industry Applications*, vol. 54, no. 1, pp. 787–795, 2018, doi: 10.1109/TIA.2017.2764875.

[39] C. Ye, H. Chan, D. Lan, P. Das, S. Sahoo, "Efficiency improvement of multichannel LED driver with selective dimming," *IEEE Transactions on Power Electronics*, vol. 35, no. 6, pp. 6280–6291, 2020, doi: 10.1109/TPEL.2019.2951629.